Environmental Science & Technology

pubs.acs.org/est

Article

Modulating Anion Nanotraps via Halogenation for High-Efficiency $^{99}TcO_4^-/ReO_4^-$ Removal under Wide-Ranging pH Conditions

Xinyi Yang,[‖] Weijin Wu,[‖] Yinghui Xie, Mengjie Hao, Xiaolu Liu, Zhongshan Chen, Hui Yang,* Geoffrey I. N. Waterhouse, Shengqian Ma,* and Xiangke Wang*

Cite This: *Environ. Sci. Technol.* 2023, 57, 10870−10881

Read Online

ACCESS | Metrics & More | Article Recommendations | Supporting Information

ABSTRACT: Efficient and sustainable methods for $^{99}TcO_4^-$ removal from acidic nuclear waste streams, contaminated water, and highly alkaline tank wastes are highly sought after. Herein, we demonstrate that ionic covalent organic polymers (iCOPs) possessing imidazolium-N^+ nanotraps allow the selective adsorption of $^{99}TcO_4^-$ under wide-ranging pH conditions. In particular, we show that the binding affinity of the cationic nanotraps toward $^{99}TcO_4^-$ can be modulated by tuning the local environment around the nanotraps through a halogenation strategy, thereby enabling universal pH $^{99}TcO_4^-$ removal. A parent iCOP-1 possessing imidazolium-N^+ nanotraps showed fast kinetics (reaching adsorption equilibrium in 1 min), a high adsorption capacity (up to 1434.1 ± 24.6 mg/g), and exceptional selectivity for $^{99}TcO_4^-$ and ReO_4^- (nonradioactive analogue of $^{99}TcO_4^-$) removal in contaminated water. By introducing F groups near the imidazolium-N^+ nanotrap sites (iCOP-2), a ReO_4^- removal efficiency over 58% was achieved in 60 min in 3 M HNO_3 solution. Further, introduction of larger Br groups near the imidazolium-N^+ binding sites (iCOP-3) imparted a pronounced steric effect, resulting in exceptional adsorption performance for $^{99}TcO_4^-$ under super alkaline conditions and from low-activity waste streams at US legacy Hanford nuclear sites. The halogenation strategy reported herein guides the task-specific design of functional adsorbents for $^{99}TcO_4^-$ removal and other applications.

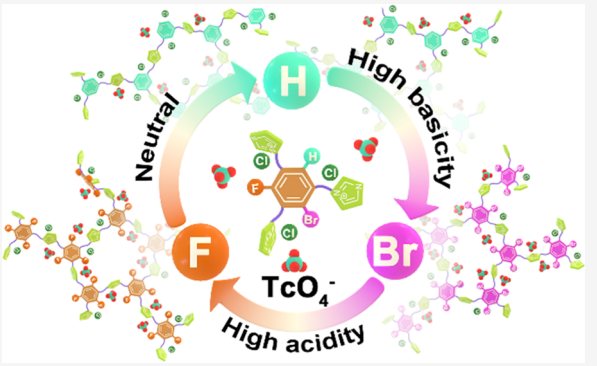

KEYWORDS: *pertechnetate, perrhenate, nuclear waste, dynamic capture, environmental remediation*

INTRODUCTION

Nuclear fission is attractive as a low-carbon electricity generation technology, and thus will likely play an important support role in the transition away from polluting fossil fuel energy.[1−3] However, the use of uranium as a nuclear fission fuel generates nuclear waste stockpiles, creating the potential for nuclear accidents and environmental catastrophes. Technetium-99 (^{99}Tc), as the fission product of ^{235}U and ^{239}Pu nuclear fuels, is one of the main radioactive nuclides in nuclear waste streams.[4−7] ^{99}Tc is a β-emitting radionuclide with a long half-life of 2.14×10^5 years. In aqueous solution, ^{99}Tc exists primarily as the pertechnetate anion ($^{99}TcO_4^-$), which possesses a high water solubility, toxicity, and environmental mobility, thereby raising environmental and ecological concerns. If $^{99}TcO_4^-$ is released into the environment, it has the potential to adversely impact entire ecosystems.[8−13] Further, upon ingestion and accumulation in the body, radioactive $^{99}TcO_4^-$ causes germ cell damage, cancer, and increased incidence of benign and malignant neoplasms in a variety of tissues and organs.[14,15] Accordingly, the selective removal of $^{99}TcO_4^-$ from nuclear waste streams or contaminated water sources has received much attention in recent years.

The selective removal of $^{99}TcO_4^-$ from nuclear waste streams or contaminated water is technically very challenging, owing to (i) strongly acidic and complex components in high-level-liquid wastes; (ii) super alkalinity of low-level activity tank waste stored at Hanford (LAW) and high-level waste at Savannah River Site (SRS);[16,17] (iii) leaking of $^{99}TcO_4^-$ from nuclear waste flows into the subsurface groundwater (high ionic strength), leading to large areas of water contamination.[8,10,11] Currently, ion exchange methods represent the most promising technology for the capture and separation of $^{99}TcO_4^-$. This approach offers easy operation and high efficiency. Commonly used ion exchange materials include resins,[7,18] molecular compounds,[19] silica,[20−22] metal borates,[23,24] layered double hydroxide (LDH),[25,26] metal−organic frameworks (MOFs),[27−38] ionic polymers,[39−46]

Received: April 19, 2023
Revised: June 20, 2023
Accepted: June 26, 2023
Published: July 11, 2023

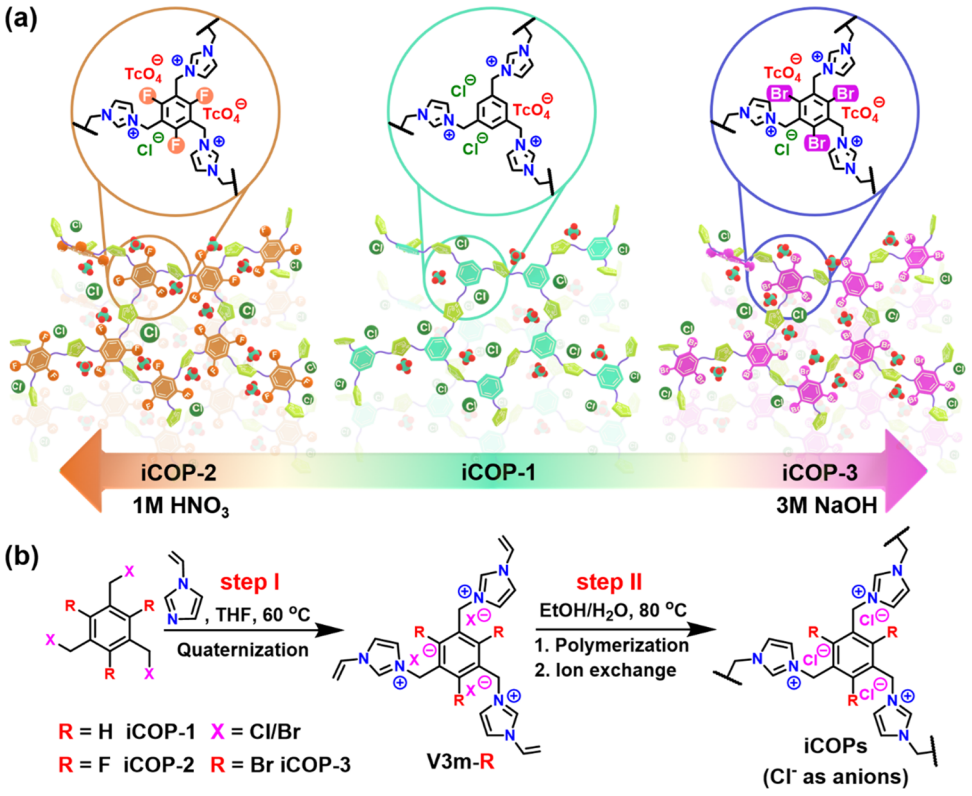

Figure 1. (a) Schematic illustration of the anion nanotraps chelation and halogenation strategy for the selective capture of $^{99}TcO_4^-$ under wide-ranging pH conditions. (b) Synthetic scheme for the synthesis of the iCOPs.

cationic covalent organic nanosheets (iCONs),[47] and covalent organic frameworks (COFs),[48−51] among others.[52] Resins, molecular compounds, and LDH-based adsorbents all have limitations due to their relatively low $^{99}TcO_4^-$ adsorption capacity and poor selectivity. Recently, MOFs and COFs have demonstrated excellent $^{99}TcO_4^-$ capture abilities, offering the advantages of a high uptake capacity, fast adsorption kinetics, and good selectivity.[27−34,36,37,47−49,51,53] Although MOFs and COFs display fast kinetics and high capacity under mild conditions, they are generally unsuitable for $^{99}TcO_4^-$ adsorption under strongly acidic, high ionic strength, or alkaline solutions due to instability issues (i.e., under conditions most relevant to the treatment of nuclear waste streams).[38,54]

In general, adsorbents differ widely in their relative affinities for $^{99}TcO_4^-$ and other competing ions. In designing adsorbents that selectively bind specific metal ions, it is important to consider both the direct adsorption site and second coordination sphere interactions.[39,55] Synergistic effects involving second coordination sphere interactions (such as hydrogen bonding or steric effects) have been shown to greatly enhance the binding affinity of adsorbents toward specific cations and anions. This adsorption site modulating principle inspired us to explore whether the adsorption selectivity of polymeric adsorbents toward $^{99}TcO_4^-$ could be tuned by introducing functional groups into the polymer framework, thereby achieving the selective adsorption of $^{99}TcO_4^-$ (and its surrogate ReO_4^-) under wide-ranging pH and ionic strengths conditions, in particular under strongly acidic and alkaline solutions.

To achieve the selective removal of $^{99}TcO_4^-$ objective under wide-ranging conditions, we herein constructed a family of ionic covalent organic polymers (iCOPs) with cationic imidazolium sites (imidazolium-N^+ anion nanotraps[39,46]) for $^{99}TcO_4^-$ binding (Figure 1a). By replacing C−H groups on the aromatic ring linkers near the imidazolium-N^+ groups in the parent polymer (iCOP-1) with F groups (iCOP-2) or Br groups (iCOP-3), it was possible to optimize the binding affinity toward $^{99}TcO_4^-$ and establish structure−property relationships. Introduction of C−F bonds gave the ionic polymer (iCOP-2) increased hydrophobicity and lower polarity, effectively preventing the adsorption of H^+ and NO_3^- at the imidazolium-N^+ anion nanotrap sites (Figure 1a), thus boosting $^{99}TcO_4^-$ adsorption selectivity under strongly acidic conditions.[56,57] Moreover, when Br groups were de novo introduced on the aromatic linkers, the obtained ionic polymer (iCOP-3) exhibited enhanced hydrophobicity and strong steric effects at the imidazolium-N^+ binding sites,[58,59] leading to the preferential adsorption of $^{99}TcO_4^-$ (and surrogate ReO_4^-) in 3 M NaOH. Subsequent experiments revealed that iCOP-3 is able to remove $^{99}TcO_4^-$ efficiently (>85% removal) from solutions relevant to Hanford low-activity waste (LAW) streams at US legacy nuclear sites. Further, iCOP-1 can dynamically and efficiently remove $^{99}TcO_4^-/ReO_4^-$ from contaminated groundwater and tap water, outperforming commercial adsorbents such as IRA-402, IRA-4200, and D311, and all other adsorbents reported thus far. Our strategy of using halogen assistants in ionic polymers is expected to stimulate widespread research into the design of high-performance adsorbents for the selective removal of anionic pollutants from aqueous systems.

https://doi.org/10.1021/acs.est.3c02967
Environ. Sci. Technol. 2023, 57, 10870−10881

MATERIALS AND METHODS

Synthesis of iCOP-1, iCOP-2, and iCOP-3. V3m-H (1.0 g, Supporting Information) and azobisisobutyronitrile (AIBN, 0.1 g) were dissolved in a mixed solvent solution containing ethanol (30 mL) and deionized H_2O (10 mL) in a 100 mL round-bottom flask. Next, the mixture was refluxed at 80 °C for 24 h under a nitrogen atmosphere. After cooling to room temperature, the product was collected by filtration, and washed several times with deionized H_2O and ethanol. The dried product is denoted herein as iCOP-1. iCOP-2 and iCOP-3 were prepared via a similar synthetic route, replacing V3m-H with V3m-F (1.0 g) or V3m-Br (1.0 g).

$^{99}TcO_4^-$ and ReO_4^- Adsorption Experiments. Caution! ^{99}Tc is a β-emitter (E_{max} = 0.29 MeV). All operations relating to the handling of this substance were performed in a licensed radiochemical laboratory.

$^{99}TcO_4^-/ReO_4^-$ Adsorption Studies. Adsorption experiments were carried out at a fixed adsorbent/liquid ratio of 0.1 g/L at 25 °C. iCOP-1 was dispersed in a solution containing ~14 ppm $^{99}TcO_4^-$. Aliquots were collected at regular time intervals while constantly stirring the dispersion. The adsorbent was collected on a 0.22 μm membrane filter, and $^{99}TcO_4^-$ in the filtrate was quantified using a liquid scintillation counting (LSC) system. A solution containing ~28 ppm ReO_4^- was used to verify the $^{99}TcO_4^-$ uptake results, with the ReO_4^- concentration in the filtrate quantified spectrophotometrically at 396 nm following reaction with the chromogenic agents KSCN and $SnCl_2{\cdot}2H_2O$ (chromogenic method).

ReO_4^- Adsorption Capacity Studies. The ReO_4^- adsorption capacity experiments were carried out at 25 °C (or 35, 45 °C). iCOP-1, iCOP-2, or iCOP-3 were added into aqueous solutions with ReO_4^- concentrations ranging from ~20 to ~250 ppm at an adsorbent/liquid ratio of 0.1 g/L. The freshly prepared dispersions were sonicated and then shaken overnight. Subsequently, the dispersions were filtered on a 0.22 μm membrane filter to remove the adsorbent, with the ReO_4^- concentration in the filtrates quantified by the chromogenic method.

Uptake Capacity Calculations. The ReO_4^- uptake capacity (q_e, mg/g) at equilibrium was calculated according to the following equation

$$q_e = \frac{(C_0 - C_e) \times V}{m}$$

where C_0 and C_e are the initial and equilibrium ReO_4^- concentrations, respectively, V is the volume of the solution, and m is the mass of the adsorbent.

Adsorption Isotherm Calculations. The isotherm data were fitted to the Langmuir model using the following equation[60]

$$\frac{C_e}{q_e} = \frac{1}{K_L q_m} + \frac{C_e}{q_m}$$

where q_e is the amount of ReO_4^- adsorbed at equilibrium and C_e is the equilibrium concentration; q_m is the maximum adsorption amount; and K_L is an equilibrium constant related to the binding strength.

Distribution Coefficient (K_d) Calculations. The K_d was calculated according to the following equation

$$K_d = \frac{(C_0 - C_e) \times V}{m \times C_e}$$

where C_0 and C_e are the initial and equilibrium ReO_4^- concentrations, respectively; V is the volume of the solution; and m is the mass of the adsorbent.

Thermodynamic Parameters Calculations. The thermodynamic parameters such as $\Delta H°$, $\Delta G°$, and $\Delta S°$ for the adsorption of ReO_4^- on the iCOPs were calculated according to the following equations

$$\ln K_d = -\frac{\Delta H°}{RT} + \frac{\Delta S°}{R}$$

$$\Delta G° = -RT \ln K_d$$

where K_d is distribution coefficient, R is the universal gas constant 8.314 J/(k·mol), T is the temperature (K); $\Delta H°$ is the standard enthalpy change, $\Delta G°$ is the standard free energy change, and $\Delta S°$ is the standard entropy change.

ReO_4^- Adsorption Kinetics Studies. The experiments were carried out at 25 °C. To determine the ReO_4^- adsorption kinetics, iCOP-1, iCOP-2, or iCOP-3 were dispersed in an aqueous solution (~pH 5.9, 1 M HNO_3, 1 M NaOH, or 3 M NaOH) containing ~28 ppm ReO_4^-. The resulting dispersion was stirred at 180 rpm, with aliquots of the dispersion being collected at regular time intervals. The aliquots were filtered through a 0.22 μm membrane filter and ReO_4^- in the filtrates was quantified by the chromogenic method.

Reusability Study. After ReO_4^- adsorption experiments, iCOP-1, iCOP-2, or iCOP-3 were immersed in 500 mL of 2 mol/L NaCl solution at 25 °C for 24 h, followed by washing with distilled water. The solid absorbents were then dried under a vacuum at 40 °C for reuse. Then, the iCOPs were subsequently returned to the aqueous solution (~pH 5.9, or 3 M NaOH) containing ~28 ppm ReO_4^- for further adsorption tests.

Anion Exchange Selectivity Study. The possible effect of competing anions on ReO_4^- adsorption was investigated by adding different concentrations of $NaNO_3$ (0.15, 1.5 mmol/L), Na_2SO_4 (0.15, 1.5 mmol/L), Na_2CO_3 (0.15, 1.5 mmol/L), NaCl (0.15, 1.5 mmol/L), or CH_3COONa (0.15, 1.5 mmol/L) into a $NaReO_4$ (0.15 mmol/L) solution. Experiments were carried out at 25 °C. iCOP-1, iCOP-2, or iCOP-3 were dispersed in the above solutions. After being stirred at a rate of 180 rpm for 12 h, the adsorbent was removed on a 0.22 μm membrane filter and the concentration of ReO_4^- in the filtrate was quantified by the chromogenic method.

$^{99}TcO_4^-$ Adsorption from Simulated Hanford Low-Activity Waste (LAW) Melter Recycle Stream. The simulated Hanford low-activity waste (LAW) melter recycle stream was prepared according to a reported protocol.[43] In addition to 1.94×10^{-4} mol/L $^{99}TcO_4^-$, the Hanford LAW stream contain large excesses of NO_3^- (6.07×10^{-2} mol/L), Cl^- (6.93×10^{-2} mol/L), NO_2^- (1.69×10^{-1} mol/L), SO_4^{2-} (6.64×10^{-6} mol/L), and CO_3^{2-} (4.3×10^{-5} mol/L) (Table S6). Adsorption experiments were carried out at a fixed adsorbent/liquid ratio of 5 g/L. After stirring for 2 h, the adsorbent was collected on a 0.22 μm membrane filter and $^{99}TcO_4^-$ in the filtrate was analyzed by a liquid scintillation counting (LSC) system.

Dynamic ReO_4^- Adsorption Studies. ReO_4^- breakthrough experiments were conducted using a laboratory-scale fixed-bed reactor at 25 °C. A mixture of iCOP-1 (40 mg) and

https://doi.org/10.1021/acs.est.3c02967
Environ. Sci. Technol. 2023, 57, 10870−10881

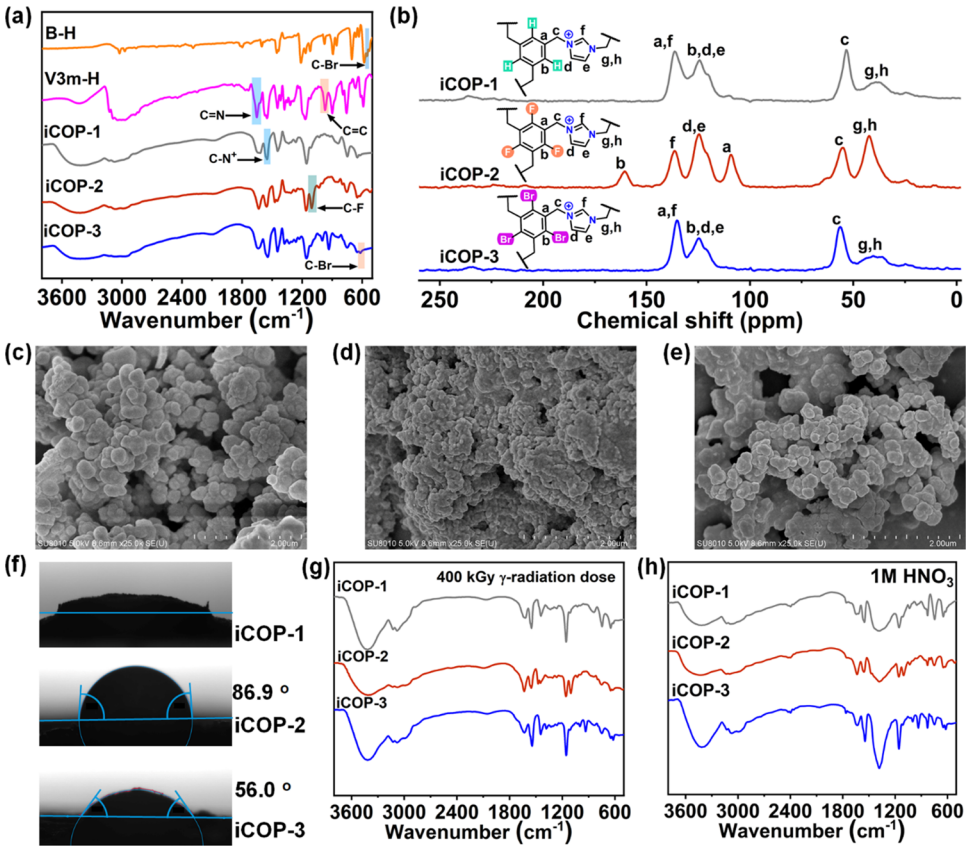

Figure 2. (a) FT-IR spectra for iCOP-1, iCOP-2, iCOP-3, V3m-H, and the 1,3,5-tris(bromomethyl)benzene (B−H) linker. (b) ^{13}C CP-MAS solid-state NMR spectra of iCOP-1, iCOP-2, and iCOP-3. (c−e) SEM images of iCOP-1, iCOP-2, and iCOP-3. (f) Water droplet contact angles on pressed pellets of iCOP-1, iCOP-2, and iCOP-3. (g, h) FT-IR spectra of iCOP-1, iCOP-2, and iCOP-3 after treatments under various conditions.

SiO_2 (160 mg) was packed into a quartz column (3.4 mm inside diameter, 1.6 mm wall thickness, 102 mm length) with degreased cotton filling the void space. Next, ReO_4^- spiked tap water or groundwater (~10 ppm) was flowed through the adsorbent column. The effluent from the adsorbent column was quantified by the chromogenic method. Under similar test conditions, 200 mg of SiO_2 was used as a blank for comparison. After the breakthrough experiments, iCOP-1 was washed with 2 mol/L NaCl solution, followed by washing with distilled water. The column was then used for the cycling test.

Dynamic Uptake Capacity Calculations. The ReO_4^- uptake capacity (q_e, mg/g) at equilibrium was calculated according to the following equation

$$q_e = \frac{\int_0^V (C_0 - C_V)\mathrm{d}V}{m}$$

where C_0 and C_V are the initial and equilibrium ReO_4^- concentrations, respectively; V is the volume of the solution; and m is the mass of the adsorbent.

RESULTS AND DISCUSSION

Material Synthesis and Characterization. The synthetic strategy used to prepare iCOP-1, iCOP-2, and iCOP-3 is shown in Figure 1b. The initial step involved building imidazolium-N^+ nanotraps with different halogen functional groups located within an ionic monomer (denoted as V3m-R, R = H, F, and Br) using a quaternization reaction (Figure 1b, step I). Proton nuclear magnetic resonance (^{1}H NMR) spectroscopy and ^{13}C NMR spectroscopy revealed the successful synthesis of the V3m-H, V3m-F, and V3m-Br monomers containing imidazolium-N^+ and vinyl groups (see Material Synthesis Section in the Supporting Information, Figures S1−S14). Fourier transform infrared (FT-IR) spectroscopy showed the disappearance of the C−Br stretching band at 549 cm^{-1} characteristic of the tris(bromomethyl)-benzene (B−H) linker and the appearance of peaks at 968 and 1647 cm^{-1} in the V3m-H, V3m-F, and V3m-Br monomers, which were assigned to vinyl C═C bending and imidazolium ring C═N stretching modes, respectively. A further new peak at ~1568 cm^{-1} is associated with an imidazolium ring C−N^+ stretching mode (Figures 2a and S15).[61] Next, the V3m-H monomer was polymerized using azobisisobutyronitrile (AIBN) as an initiator at 80 °C for 24 h, yielding iCOP-1 (Figure 1b, step II). iCOP-2 and iCOP-3 were synthesized under similar react conditions by replacing V3m-H with V3m-F or V3m-Br monomer, respectively. In a subsequent step, iCOP-1 and iCOP-3 were soaked in a 2 mol/L NaCl aqueous solution to exchange Br^- for Cl^-. This process resulted in iCOP-1, iCOP-2, and iCOP-3 all having Cl^- anions for easy comparison. The complete anion exchange (i.e., substitution of Br^- with Cl^-) was verified by X-ray photoelectron spectroscopy (XPS) analysis, with Cl signals replacing Br signals (Figure S16). The powder X-ray diffraction (PXRD) patterns for iCOP-1, iCOP-2, and iCOP-3 all exhibited a broad peak at 2θ angles around 24°, suggesting amorphous structures (Figure S17). The disappearance of vinyl C═C peak at ~968 cm^{-1} in the FT-IR spectra confirmed iCOP-1, iCOP-2, and iCOP-3 were polymeric materials (Figures 2a and S15). The C−F and

https://doi.org/10.1021/acs.est.3c02967
Environ. Sci. Technol. 2023, 57, 10870−10881

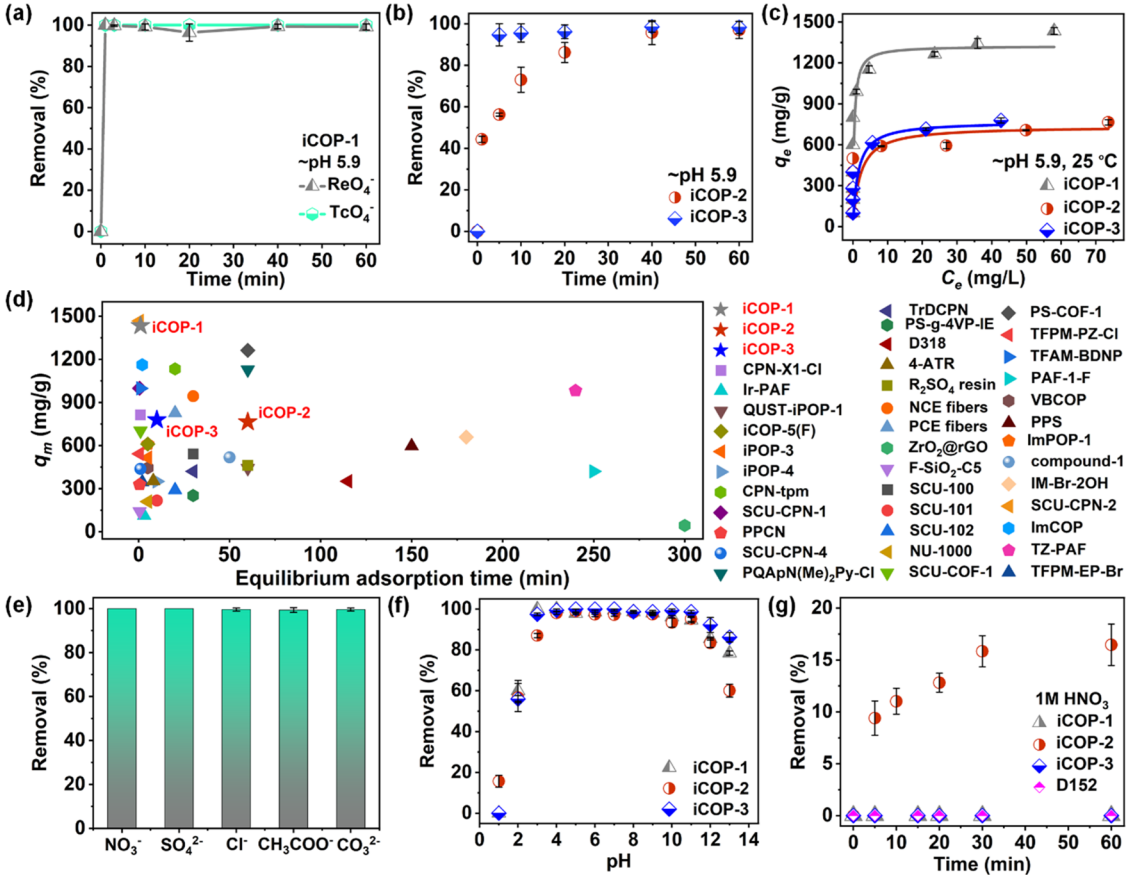

Figure 3. (a) $^{99}TcO_4^-$ and ReO_4^- adsorption kinetics on iCOP-1 at initial $^{99}TcO_4^-$ and ReO_4^- concentrations of ~14 and 28 ppm, respectively. (b) ReO_4^- adsorption kinetics on iCOP-2 and iCOP-3 at an initial ReO_4^- concentration of ~28 ppm. (c) Equilibrium adsorption isotherms for ReO_4^- on iCOP-1, iCOP-2, and iCOP-3 at 25 °C. (d) Comparison of ReO_4^- uptake amount by iCOP-1 and other reported materials. (e) Effect of possible competing anions on ReO_4^- uptake by iCOP-1 via anion exchange (ReO_4^-/other anion = 1:1). (f) Effect of initial pH on the removal of ReO_4^- by different iCOPs. (g) ReO_4^- adsorption kinetics on iCOP-1, iCOP-2, iCOP-3, and D152 in 1 M HNO_3.

C−Br groups on the aromatic ring of the linkers were retained after polymerization, evidenced by the retention of peaks at 1097 and 613 cm^{-1} for iCOP-2 and iCOP-3, respectively (Figure 2a).[62] The presence of polymeric C−C bonds in all of the iCOPs was evidenced by the appearance of signals at around 38.4 (peak h) to 42.5 (peak g) ppm in the solid-state ^{13}C cross-polarization with magic-angle spinning (CP-MAS) NMR spectra, confirming the success of the vinyl addition polymerization (Figure 2b). Moreover, the ^{13}C CP-MAS solid-state NMR spectra of iCOPs-1, 2, and 3 showed signals at ~60 ppm attributed to C−imidazolium−N^+ bonds, consistent with the FT-IR results.[63] The C−F and C−Br groups were also identified in the ^{13}C NMR spectra, and thus could be used to "fingerprint" iCOP-2 (C−F, 160 ppm, peak b) and iCOP-3 (C−Br, 125 ppm, peak b) (Figure 2b).[64,65] Scanning electron microscopy (SEM) revealed similar nanosphere morphologies for iCOP-1, iCOP-2, and iCOP-3 (Figure 2c−e). The surface wettability properties of the iCOPs were studied by water droplet contact angle measurements. The water droplets were rapidly absorbed by iCOP-1, indicating good hydrophilicity (Figure 2f). In contrast, the F and Br functional groups in iCOP-2 and iCOP-3 imparted hydrophobicity with water contact angles of 86.9 and 56.0°, respectively.

Next, we checked the radiation resistance properties of iCOPs by exposing the samples to γ-ray irradiation. Post-treatment FT-IR spectra confirmed the integrity of the ionic polymers after 400 kGy γ-ray dose (Figure 2g). The chemical stabilities of the iCOPs were initially evaluated by soaking the samples in the HNO_3 (1 M) and NaOH (3 M) solutions for 72 h. FT-IR spectra of the treated samples showed no obvious changes after immersion in 1 M HNO_3, suggesting excellent acid stability (Figure 2h).[44] iCOP-2 and iCOP-3 also showed good stability after treatment in 3 M NaOH (Figure S18). For iCOP-1, a significant decrease in the intensity of the imidazolium-N^+ signal at 1568 cm^{-1} in the FT-IR spectrum was observed following the NaOH treatment (Figure S18), suggesting some changes in the chemical structure of iCOP-1. This superior stability of iCOP-2 and iCOP-3 can be attributed to the F and Br groups on the aromatic linkers, which increased the hydrophobicity of the polymers (thus likely preventing hydroxide ions from attacking the imidazolium-N^+ sites, therefore improving the chemical stability under high alkalinity conditions). Thermogravimetric (TGA) analyses on iCOP-1, iCOP-2, and iCOP-3 showed no obvious weight loss with heating of the samples up to 300 °C, implying good thermal stability (Figure S19).

The imidazolium-N^+ nanotraps on the iCOPs were expected to offer an abundance of accessible binding sites for anions such as pertechnetate and perrhenate in an aqueous solution. We hypothesized that the close proximity of the halogen functional groups to the imidazolium-N^+ nanotraps would affect the binding strengths of different anions with the nanotrap binding sites, thereby enhancing the adsorption selectivity toward pertechnetate and perrhenate ions. As a

https://doi.org/10.1021/acs.est.3c02967
Environ. Sci. Technol. 2023, 57, 10870−10881

proof of concept, the adsorption efficiencies of the iCOP-1, iCOP-2, and iCOP-3 for $^{99}TcO_4^-/ReO_4^-$ capture were evaluated under wide-ranging conditions, with our experimental and computational findings below fully validating our hypothesis.

$^{99}TcO_4^-/ReO_4^-$ Capture Performance. Initially, the $^{99}TcO_4^-$ adsorption properties of iCOP-1 were evaluated in an ~14 ppm aqueous solution (~pH 5.9). As shown in Figure 3a, iCOP-1 showed very fast adsorption kinetics with a removal ratio of over 99.9% in 1 min at an adsorbent/liquid ratio of 0.1 g/L. Owing to the scarcity of the purified $^{99}TcO_4^-$ and its high radioactivity, subsequent adsorption experiments were performed using ReO_4^- (as a nonradioactive surrogate for $^{99}TcO_4^-$). ReO_4^- possesses a structure, charge density, and water solubility very similar to $^{99}TcO_4^-$, making it a near-ideal surrogate.[5] Adsorption experiments on iCOP-1 were subsequently performed in an ~28 ppm ReO_4^- aqueous solution (~pH 5.9). As expected, the adsorption kinetics for ReO_4^- were almost identical to those of $^{99}TcO_4^-$ under the same conditions (Figure 3a). Encouraged by these results, the nonradioactive ReO_4^- surrogate was used for subsequent adsorption studies. In comparison to iCOP-1, for which >99.9% removal of ReO_4^- was realized in 1 min, iCOP-2 and iCOP-3 demonstrated relatively slow ReO_4^- adsorption kinetics under similar conditions (~pH 5.9, Figure 3b). For iCOP-2 and iCOP-3, 97.0 ± 4.1 and 95.6 ± 4.4% ReO_4^- removal was achieved after 60 and 10 min, respectively.

Next, equilibrium adsorption data were collected to determine the adsorption capacity of the iCOPs at 25 °C. An adsorbent-to-liquid ratio of 0.1 g/L was determined to be suitable for each iCOP (Figure S20) and used for subsequent adsorption studies. For the equilibrium adsorption studies, the ReO_4^- concentration was varied from ~20 to ~250 ppm at an adsorbent/liquid ratio of 0.1 g/L. The adsorption capacities were 1434.1 ± 24.6, 764.6 ± 19.9, and 778.4 ± 18.5 mg/g for iCOP-1, iCOP-2 (F functional groups), and iCOP-3 (Br functional groups), respectively (Figure 3c and, Tables S1 and S2). The extraction capacity of iCOP-1 exceeded commercial IRA-402, IRA-4200, D101, D311, celite, and hydrotalcite, and all reported other sorbents thus far, except for SCU-CPN-2 (1467 mg/g)[45] (Figures 3d and S21, and Table S1). The calculated distribution coefficient (K_d) of iCOP-1 is 1.0×10^6 mL/g, comparable to other high-performance adsorbents reported in the literature, such as SCU-100 (1.9×10^5 mL/g),[29] SCU-COF-1 (3.9×10^5 mL/g),[54] and VBCOP (4.0×10^5 mL/g),[44] suggesting an excellent binding affinity for ReO_4^-. We performed further equilibrium adsorption experiments at 35 and 45 °C to determine the thermodynamic parameters of ReO_4^- adsorption. The experimental and calculated results are summarized in Figure S22. Accordingly, the calculated the standard free energy change ($\Delta G°$) for ReO_4^- adsorption on iCOP-1, iCOP-2, and iCOP-3 ranged from −17.25 to −10.40 kJ/mol, suggesting a spontaneous sorption process (Table S3). The standard entropy change ($\Delta S°$) and enthalpy change ($\Delta H°$) for ReO_4^- adsorption on iCOP-1 were −231.33 J/K/mol and −84.67 kJ/mol, implying that the system became more ordered after adsorption with the adsorption process being exothermic. For iCOP-2 and iCOP-3, the $\Delta H°$ values were positive, indicating an endothermic sorption process.

The excellent performance of iCOP-1 for ReO_4^- adsorption at pH 5.9 encouraged us to assess the ion exchange selectively against other competing anions, such as NO_3^-, SO_4^{2-}, Cl^-, CH_3COO^-, and CO_3^{2-}. The relative ReO_4^- removal efficiency in the presence of these common anions was >99.9, >99.9, 99.6 ± 0.7, 99.4 ± 1.1, and 99.6 ± 0.7%, respectively (Figure 3e). Subsequent studies confirmed the remarkably high selectivity of iCOP-1 toward ReO_4^- over these other anions, even when the other anions were in a 10-fold concentration relative to ReO_4^-. The number of imidazolium-N^+ binding sites was calculated to be $\sim 3.53 \times 10^{21}$, higher than the number of ReO_4^- ions in the sample solution ($\sim 1.81 \times 10^{20}$). The number of each other anions such as NO_3^-, SO_4^{2-}, Cl^-, CH_3COO^-, or CO_3^{2-} was 10-fold higher ($\sim 1.81 \times 10^{21}$). The results revealed that the iCOP-1 maintained a very strong affinity toward ReO_4^- even under high ionic strength conditions (Figure S23). iCOP-2 and iCOP-3 showed similar high selectivity for ReO_4^- under the same conditions (Figure S24). Durability and cycling stability are further important considerations for practical adsorbents. We thus determined the durability and cyclic stability of iCOPs under various conditions. The ReO_4^- adsorption kinetics and removal efficiency of iCOP-1 were almost unchanged after 400 kGy γ-radiation dose (Figures S25 and S26). After γ-radiation treatment, the adsorption capacities of iCOP-1, iCOP-2, and iCOP-3 were determined to be 1408, 768, and 728 mg/g, respectively, confirming their excellent radiation stability (Figure S25). SEM images showed that iCOP-1, iCOP-2, and iCOP-3 retained their initial nanosphere morphologies after ReO_4^- adsorption (Figure S27). The ReO_4^- exchanged iCOP-1 could readily be regenerated by elution with a NaCl solution, with an adsorption efficiency >86% maintained over five cycles (Figure S28).

Next, the ReO_4^- adsorption abilities of the different iCOPs were determined at pH values ranging from 1 to 13. The ReO_4^- removal efficiencies of iCOP-1, iCOP-2, and iCOP-3 were similar at pH values between 4 and 11 (Figure 3f). It is worth mentioning that iCOP-2 and iCOP-3 showed the best ReO_4^- adsorption performance at pH 1 and 13, respectively. Given the different ReO_4^- removal efficiencies of iCOP-1, iCOP-2, and iCOP-3 under low and high pH values ($pH \leq 2$ and $pH \geq 12$), we postulated that a high density of imidazolium-N^+ nanotraps is the fundamental factor influencing the ReO_4^- binding affinity of the iCOPs, with the nearby halogen sites (such as F and Br) affecting the ReO_4^- binding strength.

The strongly acidic high-level liquid wastes and super alkaline tank wastes stored at Hanford and Savannah River Sites represent a significant obstacle to the design of adsorbents for $^{99}TcO_4^-$ capture.[16,17] Our results revealed that iCOP-2 showed relatively high ReO_4^- removal efficiency at pH 1, while iCOP-3 demonstrated excellent ReO_4^- removal performance at high pH (12 and 13) values, prompting evaluation of their adsorption performance under strongly acidic and strongly basic conditions. The ReO_4^- adsorption ability of iCOPs was first determined in 1 M HNO_3 solutions. Figures 3g and S29, and Table S4 revealed that approx. 16.5 ± 2.0, 61, and 81% of the available ReO_4^- were extracted by iCOP-2 at adsorbent-to-solution ratios of 2, 20, and 40 g/L, respectively, exceeding the performance of a commercial polymer sorbent D152, D311, IRA-4200, IRA-402, and most previously reported adsorbents. The adsorption capacity of iCOP-1 and iCOP-3 were <0.1 mg/g under such strongly acidic conditions. In addition, iCOP-2 could remove over 58% of ReO_4^- from 3 M HNO_3 solution (28 ppm ReO_4^-) at an adsorbent-to-liquid ratio of 60 g/L (superior to commercial

https://doi.org/10.1021/acs.est.3c02967
Environ. Sci. Technol. 2023, 57, 10870−10881

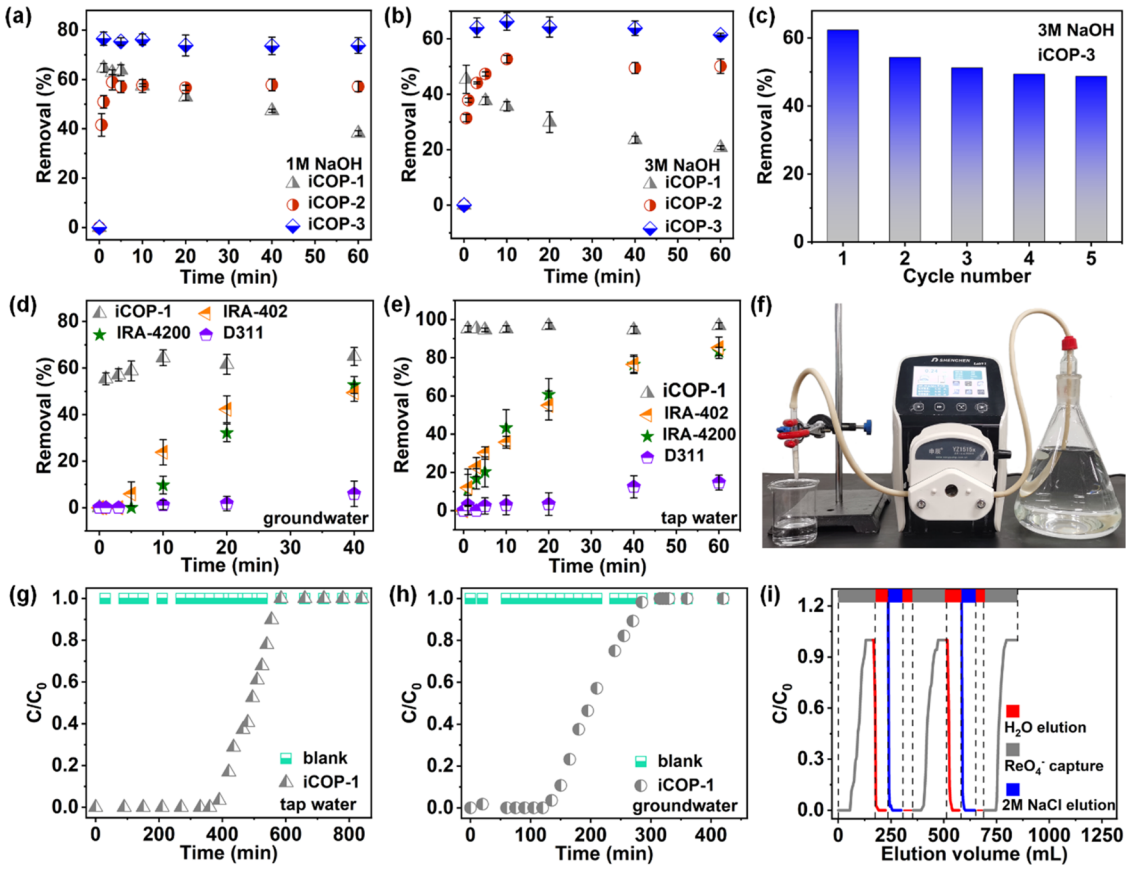

Figure 4. (a) ReO_4^- adsorption kinetics on iCOP-1, iCOP-2, and iCOP-3 in 1 M NaOH. (b) ReO_4^- adsorption kinetics on iCOP-1, iCOP-2, and iCOP-3 in 3 M NaOH. (c) Recycle test data for ReO_4^- removal in 3 M NaOH. (d) ReO_4^- adsorption kinetics on iCOP-1, D311, IRA-402, and IRA-4200 in spiked groundwater. (e) ReO_4^- adsorption kinetics on iCOP-1, D311, IRA-402, and IRA-4200 in spiked tap water. (f) Equipment used for ReO_4^- removal from groundwater and tap water by iCOP-1. (g, h) Experimental column breakthrough curves for ReO_4^- spiked groundwater and tap water in an absorber bed packed with iCOP-1. (i) Recycle test data for ReO_4^- removal in tap water (an absorber bed packed with iCOP-1).

polymer sorbents D152, D311, IRA-4200, IRA-402), performance on par or surpassing the best adsorbents previously reported (Table S4 and Figure S29).

We next carried out ReO_4^- adsorption experiments in NaOH solutions. iCOP-3 demonstrated faster adsorption kinetics than the other iCOPs, achieving an equilibrium removal percentage of 73.8 ± 3.2 and 61.4 ± 0.6% in 1 M and 3 M NaOH solutions, respectively (Figure 4a,b and Table S5). Adsorption performance was next determined in 3 M NaOH at an adsorbent-to-solution ratio of 5 g/L. Remarkably, 89% ReO_4^- removal was observed in only 10 min (Table S5 and Figure S30). To our knowledge, iCOP-3 offers a high extraction efficiency, comparable to other polymer adsorbents and commercial polymer sorbents (D152, D311, IRA-4200, IRA-402) under such extreme basic conditions (Table S5 and Figure S30). iCOP-1 and iCOP-2 showed lower ReO_4^- removal ratios under alkaline conditions. It is worth noting that the adsorption curve of iCOP-1 showed a sharp initial ReO_4^- removal rate, with the ReO_4^- uptake then decreasing over time. This is due to the collapse of its polymeric structure under harsh alkaline conditions, which was confirmed by FT-IR spectroscopy and a significant mass loss after the ReO_4^- adsorption experiments (Figures S31 and S32).

Further, we simulated the Hanford low-activity waste melter recycle stream to assess the $^{99}TcO_4^-$ extraction ability of iCOP-3.[16,39,66] The amount of anions (including NO_3^-, NO_2^-, and Cl^-) in the recycle stream is 300 times higher than that of $^{99}TcO_4^-$ (Table S6). Notably, approx. 85% of the $^{99}TcO_4^-$ was removed at an adsorbent-to-solution ratio of 5 g/L under such extreme conditions, which is comparable to other state-of-the-art adsorbents. iCOP-3 retained good regeneration performance in 3 M NaOH. Even after five adsorption/desorption cycles, the removal efficiency was reduced by only 10% (Figure 4c). FT-IR spectra revealed the chemical composition of iCOP-3 was retained after the recycling test in 3 M NaOH (Figure S33). The good chemical stability, excellent radiation stability, high elution efficiency, and easy separation from the treatment medium highlight the great potential of the iCOPs for $^{99}TcO_4^-$ extraction from nuclear waste.

Due to the high environmental mobility of $^{99}TcO_4^-$, leaked $^{99}TcO_4^-$ quickly moves into groundwater where it poses a serious threat to aquatic life and humans. Encouraged by the high adsorption capacity, fast kinetics, and good selectivity of iCOP-1 at near-neutral pH, dynamic ReO_4^- capture breakthrough experiments using spiked groundwater and tap water were conducted to simulate the treatment of contaminated water sources. Initially, the kinetics of ReO_4^- uptake on iCOP-1 in ReO_4^--spiked groundwater and tap water were studied. Commercial IRA-402, IRA-4200, and D311 were used for comparison purposes. iCOP-1 exhibited fast ReO_4^- uptake kinetics, reaching adsorption equilibrium within 5 and 1 min in groundwater and tap water, respectively (Figure 4d,e). All of

https://doi.org/10.1021/acs.est.3c02967
Environ. Sci. Technol. 2023, 57, 10870−10881

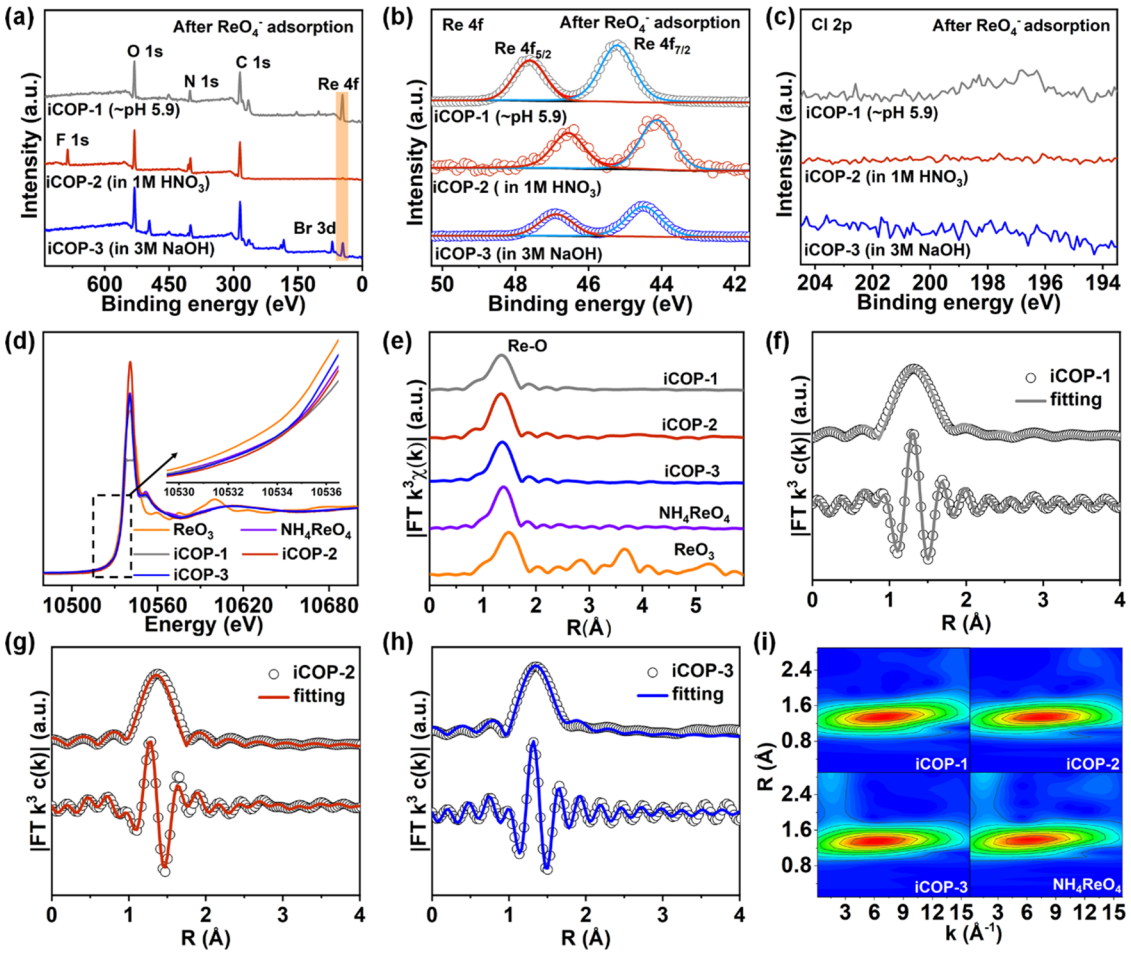

Figure 5. (a–c) XPS survey spectra for iCOP-1, iCOP-2, and iCOP-3 after ReO_4^- adsorption studies. (d) Re L_3-edge XANES spectra for iCOP-1, iCOP-2, and iCOP-3 after ReO_4^- adsorption studies. (e) Re L_3-edge EXAFS spectra in *R*-space for iCOP-1, iCOP-2, and iCOP-3 after ReO_4^- adsorption studies. (f–h) Re L_3-edge EXAFS fitting curve for iCOP-1, iCOP-2, and iCOP-3 after ReO_4^- adsorption studies. (i) Wavelet transform contour plots for iCOP-1, iCOP-2, and iCOP-3 after ReO_4^- adsorption studies. ReO_3 and NH_4ReO_4 were employed as reference materials.

the commercial adsorbents showed much slower adsorption kinetics under the same conditions. Next, we examined the dynamic adsorption performance of iCOP-1 through breakthrough experiments (Figure 4f–i). As shown in Figure 4g, iCOP-1 can effectively capture ReO_4^- from tap water, under slow column elution conditions (0.2 mL/min) reaching equilibrium after ~580 min. The calculated dynamic adsorption capacity reached as high as 24.2 mg/g. The breakthrough time for ReO_4^- in groundwater using iCOP-1 was approx. 5 h (300 min), with the equilibrium dynamic capacity being 10.6 mg/g. The lower equilibrium dynamic capacity in groundwater is due to the higher ionic strength and more complex composition of groundwater compared to tap water (Figure 4h). Significantly, the ion exchange process was completely reversible, with the adsorbed ReO_4^- able to be easily eluted using 2 mol/L NaCl solutions with negligible subsequent changes in ReO_4^- uptake (Figure 4i). The long breakthrough time, high dynamic capacity, and reusability suggest that iCOP-1 is a very promising adsorbent for use in packed columns for $^{99}TcO_4^-$ capture from contaminated water sources.

Adsorption Mechanism. After demonstrating the excellent $^{99}TcO_4^-/ReO_4^-$ extraction performance of the iCOPs in acidic, near-neutral, and alkaline media, we next sought an in-depth understanding of the $^{99}TcO_4^-/ReO_4^-$ adsorption mechanism by carrying out XPS, X-ray absorption fine structure (XAFS), and molecular dynamics (MD) simulations. The appearance of Re(VII) peaks and the complete disappearance of chloride peaks in XPS spectra of iCOP-1, iCOP-2, and iCOP-3 after the saturation ReO_4^- adsorption experiments indicated that ReO_4^- adsorption occurred by ion exchange (Figures 5a–c and S16). Compared with iCOP-1, the Re $4f_{7/2}$ and Re $4f_{5/2}$ signals for iCOP-2 and iCOP-3 were shifted to lower binding energies, which is attributed to synergistic effects between the imidazolium-N^+ sites and adjacent F or Br groups, which acted to increase the electron density on the adsorbed ReO_4^- anions.[40,41]

Re L_3-edge X-ray absorption fine spectroscopy (XAFS) was applied to further probe the electronic structure of adsorbed ReO_4^- and to gain deeper insights into the binding sites on the iCOPs. The normalized Re L_3-edge X-ray absorption near-edge structure (XANES) spectra showed that the absorption edge position for ReO_4^- adsorbed on iCOP-1, iCOP-2, and iCOP-3 was similar to that of NH_4ReO_4 (higher than Re(VI)O_3 reference), providing further evidence that Re was present in +7 oxidation state, consistent with the XPS data (Figure 5d). The corresponding Re L_3-edge *R*-space extended XAFS (EXAFS) spectra are shown in Figure 5e. All three samples showed only one main peak at ca. 1.35 Å, which was again close to that of the NH_4ReO_4 reference. The EXAFS data

https://doi.org/10.1021/acs.est.3c02967
Environ. Sci. Technol. 2023, 57, 10870−10881

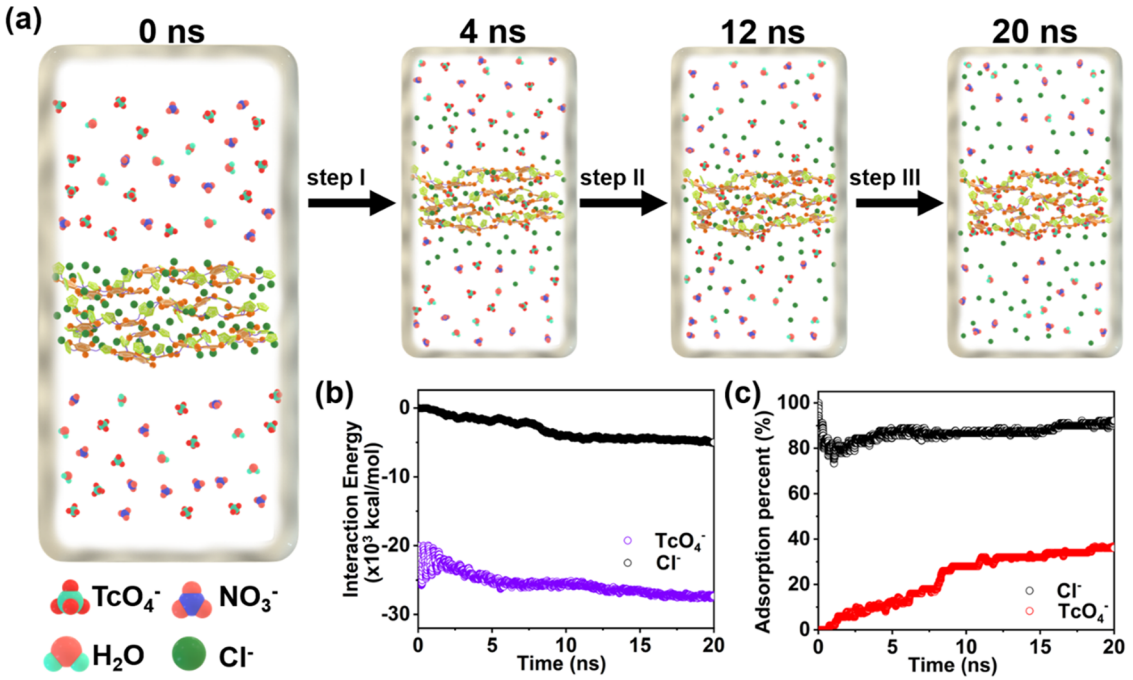

Figure 6. (a) Selected snapshots from the molecular dynamics simulation showing the anion exchange process (TcO_4^- replacing Cl^-) on iCOP-2 in HNO_3 solution. (b) Time evolution of the nonbonded interaction energies. (c) Time evolution of the adsorption ratio TcO_4^- over Cl^- anions.

could be fitted well using a Re−O scattering path, suggesting adsorption as the ReO_4^- anion (Figure 5f−h and Table S7). As expected, all three samples exhibited only one intensity maximum around 6.68 $Å^{-1}$ in k space (≈1.35 in R space) associated with Re−O and a Re(VII) oxidation state (Figure 5i).

Next, we explored the adsorption dynamics of $^{99}TcO_4^-$ on iCOP-2 in HNO_3 solutions by using molecular dynamics (MD) simulations. Since the anion exchange processes occur at the positively charged imidazolium-N^+ sites, we considered all possible affinity contributions from surrounding atoms and ions. At the beginning of the ion exchange process, Cl^- anions are located at the imidazolium-N^+ sites (Figure 6a). Subsequently, $^{99}TcO_4^-$ anions are adsorbed at the imidazolium-N^+ sites of iCOP-2 within a very short period of time, displacing Cl^- anions which move away from the binding sites (Figure 6a, step I). No NO_3^- anion adsorption was observed after ∼4 ns, with iCOP-2 displaying an extraordinary affinity for $^{99}TcO_4^-$ (a high uptake capacity and selectivity) at 12 ns even at high concentrations of NO_3^- (Figure 6a, step II). At 20 ns, the adsorbed anion ratio $^{99}TcO_4^-/Cl^-$ on iCOP-2 was >4 (36.4% $^{99}TcO_4^-$ vs 7.8% of Cl^-), suggesting a remarkable binding affinity toward $^{99}TcO_4^-$ in the HNO_3 solution (Figure 6a, step III). The binding free energy diagrams for $^{99}TcO_4^-$/iCOP-2 and Cl^-/iCOP-2 during the MD simulation are compared in Figure 6b. The calculated binding free energy of $^{99}TcO_4^-$/iCOP-2 decreased from -19.8×10^3 kcal/mol to approx. -27.3×10^3 kcal/mol (interaction energy around -7.5×10^3 kcal/mol) during the adsorption process, suggesting a strong interaction. Over the same period, the direct interaction energy between Cl^- and iCOP-2 increased by 4.9×10^3 kcal/mol (from −0 to -4.9×10^3 kcal/mol), being lower than $^{99}TcO_4^-$/iCOP-2, thus demonstrating that iCOP-2 had a relatively low affinity for Cl^-. Figure 6c shows a plot of the adsorption percentage of $^{99}TcO_4^-$ against mole fraction of Cl^- during the dynamics simulations, further indicating the excellent $^{99}TcO_4^-$ adsorption ability of iCOP-2. The desorption date, spectroscopic data, MD simulations, and interaction energy results confirm the outstanding adsorption performance of the iCOPs toward $^{99}TcO_4^-$ under wide-ranging pH conditions.

Taken together, the above results validate our general design strategy that involves introducing halogen functional groups into ionic covalent polymers to enhance $^{99}TcO_4^-$ and ReO_4^- adsorption under diverse conditions. The binding affinity between imidazolium-N^+ nanotrap and $^{99}TcO_4^-/ReO_4^-$ was shown to be sensitive to the local environment. In recent notable contributions, imidazolium-N^+ sites were found to be more favorable for the adsorption of $^{99}TcO_4^-/ReO_4^-$ compared to other common anions, including NO_3^-, Cl^-, CH_3COO^-, CO_3^{2-}, and SO_4^{2-} under mild conditions due to the higher binding free energies at imidazolium-N^+ sites.[46] Our results lend further support to these findings, with the iCOP-1 offering fast adsorption kinetics, a high uptake capacity, and good selectivity for the capture of $^{99}TcO_4^-/ReO_4^-$ in the absence of any halogen decoration. As a proof of concept, when the F or Br functional groups were introduced near the imidazolium-N^+ sites, the ionic covalent polymers showed significantly enhanced hydrophobicity and chemical stability, with the halogen groups also imparting shielding effects and steric hindrance due to their high electronegativity, weak polarizability, and size. The enhanced hydrophobicity effectively prevented H_3O^+, Cl^-, OH^-, and NO_3^- ions from adsorbing at the imidazole imidazolium-N^+ binding sites, therefore improving the binding affinity toward $^{99}TcO_4^-/ReO_4^-$. We further identified the functional relationship between the halogen-assisted imidazolium-N^+ sites and their adsorption performance. Our work demonstrates that it is possible to modulate the binding affinity of ionic covalent polymers for specific targets under specific conditions by directly tuning the local environment of binding sites through a

https://doi.org/10.1021/acs.est.3c02967
Environ. Sci. Technol. 2023, 57, 10870−10881

halogen modification. Such versatility guides the synthesis of improved adsorbents for target applications.

ENVIRONMENTAL IMPLICATIONS

Nuclear wastes include sludges and supernatant liquids containing the toxic β-emitting radionuclide technetium-99 (^{99}Tc). Concerns about the potentially hazardous impact of ^{99}Tc on the environment motivate the development of new technologies for removing the radionuclide from water and sludges. In this work, a family of ionic covalent organic polymer adsorbents for $^{99}TcO_4^-$ were rationally designed based on imidazolium-N^+ adsorption sites and halogen assistant groups for nuclear waste management. The introduction of F and Br groups in close proximity to the imidazolium-N^+ sites of the iCOPs had a significant effect on their $^{99}TcO_4^-/ReO_4^-$ adsorption and separation characteristics. The F assistant groups enhanced hydrophobicity and improved the binding affinity of imidazolium-N^+ sites for $^{99}TcO_4^-/ReO_4^-$ adsorption under strong acidic conditions, while Br created steric hindrance that improved the binding strength of the anions at imidazolium-N^+ sites in alkaline solution. The developed iCOPs-1, 2, and 3 adsorbents showed excellent radiation stability, fast adsorption kinetics, high adsorption capacities, and $^{99}TcO_4^-/ReO_4^-$ selectivity, and good reusability under wide-ranging conditions. Specifically, (i) iCOP-1 without any halogen assistant groups showed excellent potential for the dynamic removal of $^{99}TcO_4^-/ReO_4^-$ from contaminated groundwater, tap water, and other near-neutral media. (ii) Fluoro groups in iCOP-2 enhanced $^{99}TcO_4^-/ReO_4^-$ uptake in 1 M HNO_3 solution, thereby offering promise for removing $^{99}TcO_4^-$ in acidic nuclear waste streams. (iii) iCOP-3 containing bromo groups is able to rapidly remove $^{99}TcO_4^-/ReO_4^-$ from alkaline nuclear waste streams. Taken together, this work offers a versatile platform for nuclear waste management and environmental remediation, particularly for the separation of $^{99}TcO_4^-$ under extreme conditions.

ASSOCIATED CONTENT

Supporting Information

The Supporting Information is available free of charge at https://pubs.acs.org/doi/10.1021/acs.est.3c02967.

Chemicals, additional experimental procedures, and additional materials characterization data (^{1}H NMR, ^{13}C NMR, FT-IR, PXRD, TGA, SEM, photographs of samples, XPS, XAS; simulation details and methodology, adsorption calculations, and $^{99}TcO_4^-/ReO_4^-$ performance comparison) (PDF)

AUTHOR INFORMATION

Corresponding Authors

Hui Yang − *College of Environmental Science and Engineering, North China Electric Power University, Beijing 102206, P. R. China;* orcid.org/0000-0002-6745-642X; Email: h.yang@ncepu.edu.cn

Shengqian Ma − *Department of Chemistry, University of North Texas, Denton, Texas 76201, United States;* orcid.org/0000-0002-1897-7069; Email: shengqian.ma@unt.edu

Xiangke Wang − *College of Environmental Science and Engineering, North China Electric Power University, Beijing 102206, P. R. China;* orcid.org/0000-0002-3352-1617; Email: xkwang@ncepu.edu.cn

Authors

Xinyi Yang − *College of Environmental Science and Engineering, North China Electric Power University, Beijing 102206, P. R. China*

Weijin Wu − *College of Environmental Science and Engineering, North China Electric Power University, Beijing 102206, P. R. China*

Yinghui Xie − *College of Environmental Science and Engineering, North China Electric Power University, Beijing 102206, P. R. China*

Mengjie Hao − *College of Environmental Science and Engineering, North China Electric Power University, Beijing 102206, P. R. China*

Xiaolu Liu − *College of Environmental Science and Engineering, North China Electric Power University, Beijing 102206, P. R. China*

Zhongshan Chen − *College of Environmental Science and Engineering, North China Electric Power University, Beijing 102206, P. R. China*

Geoffrey I. N. Waterhouse − *School of Chemical Sciences, The University of Auckland, Auckland 1142, New Zealand;* orcid.org/0000-0002-3296-3093

Complete contact information is available at: https://pubs.acs.org/10.1021/acs.est.3c02967

Author Contributions

‖X.Y. and W.W. contributed equally to this work. All authors have given approval to the final version of the manuscript.

Notes

The authors declare no competing financial interest.

ACKNOWLEDGMENTS

The authors gratefully acknowledge funding support from the National Science Foundation of China (Grants U2167218; 22006036; 22276054), the Beijing Outstanding Young Scientist Program (H.Y., Z.C., and X.W.), and the Robert A. Welch Foundation (B-0027) (SM). G.I.N.W. was supported by a James Cook Research Fellowship from New Zealand Government funding, administered by the Royal Society Te Apārangi. The authors also acknowledge support from the 14W station in Shanghai Synchrotron Radiation Facility (SSRF).

REFERENCES

(1) Taylor, R. Reaction: A Role for Actinide Chemists. *Chem* **2016**, *1*, 662−663.

(2) Deutch, J. Is Net Zero Carbon 2050 Possible? *Joule* **2020**, *4*, 2237−2240.

(3) Gilbert, A. Q.; Bazilian, M. D. Can Distributed Nuclear Power Address Energy Resilience and Energy Poverty? *Joule* **2020**, *4*, 1839−1843.

(4) Banerjee, D.; Kim, D.; Schweiger, M. J.; Kruger, A. A.; Thallapally, P. K. Removal of TcO_4^- Ions from Solution: Materials and Future Outlook. *Chem. Soc. Rev.* **2016**, *45*, 2724−2739.

(5) Darab, J. G.; Smith, P. A. Chemistry of Technetium and Rhenium Species during Low-Level Radioactive Waste Vitrification. *Chem. Mater.* **1996**, *8*, 1004−1021.

(6) Icenhower, J. P.; Qafoku, N. P.; Zachara, J. M.; Martin, W. J. The Biogeochemistry of Technetium: A Review of the Behavior of an Artificial Element in the Natural Environment. *Am. J. Sci.* **2010**, *310*, 721−752.

(7) Xiao, C.; Khayambashi, A.; Wang, S. Separation and Remediation of $^{99}TcO_4^-$ from Aqueous Solutions. *Chem. Mater.* **2019**, *31*, 3863−3877.
(8) del Cul, G. D.; Bostick, W. D.; Trotter, D. R.; Osborne, P. E. Technetium-99 Removal from Process Solutions and Contaminated Groundwater. *Sep. Sci. Technol.* **1993**, *28*, 551−564.
(9) Amendola, V.; Bergamaschi, G.; Boiocchi, M.; Alberto, R.; Braband, H. Fluorescent Sensing of ^{99}Tc Pertechnetate in Water. *Chem. Sci.* **2014**, *5*, 1820−1826.
(10) Seliman, A. F.; Samadi, A.; Husson, S. M.; Borai, E. H.; DeVol, T. A. Preparation of Polymer-Coated, Scintillating Ion-Exchange Resins for Monitoring of ^{99}Tc in Groundwater. *Anal. Chem.* **2011**, *83*, 4759−4766.
(11) Eagling, J.; Worsfold, P. J.; Blake, W. H.; Keith-Roach, M. J. Mobilization of Technetium from Reduced Sediments Under Seawater Inundation and Intrusion Scenarios. *Environ. Sci. Technol.* **2012**, *46*, 11798−11803.
(12) Wilmarth, W. R.; Lumetta, G. J.; Johnson, M. E.; Poirier, M. R.; Thompson, M. C.; Suggs, P. C.; Machara, N. P. Review: Waste-Pretreatment Technologies for Remediation of Legacy Defense Nuclear Wastes. *Solvent Extr. Ion Exch.* **2011**, *29*, 1−48.
(13) Murphy, C. E., Jr.; Johnson, T. L. Vegetative Uptake of Technetium-99 from Buried, Solidified, Low-Level Radioactive Waste. *J. Environ. Qual.* **1993**, *22*, 793−799.
(14) Lecina, J.; Cortés, P.; Llagostera, M.; Piera, C.; Suades, J. New Rhenium Complexes with Ciprofloxacin as Useful Models for Understanding the Properties of [^{99m}Tc]-Ciprofloxacin Radiopharmaceutical. *Bioorg. Med. Chem.* **2014**, *22*, 3262−3269.
(15) Boggs, M. A.; Minton, T.; Dong, W.; Lomasney, S.; Islam, M. R.; Gu, B.; Wall, N. A. Interactions of Tc(IV) with Humic Substances. *Environ. Sci. Technol.* **2011**, *45*, 2718−2724.
(16) King, W. D.; Hassan, N. M.; McCabe, D. J.; Hamm, L. L.; Johnson, M. E. Technetium Removal from Hanford and Savannah River Site Actual Tank Waste Supernates with Superlig 639 Resin. *Sep. Sci. Technol.* **2003**, *38*, 3093−3114.
(17) DiPrete, D. P.; DiPrete, C. C.; Sigg, R. A. Measurement of ^{99}Tc in Savannah River Site High Activity Waste. *J. Radioanal. Nucl. Chem.* **2005**, *263*, 593−598.
(18) Long, K. M.; Goff, G. S.; Ware, S. D.; Jarvinen, G. D.; Runde, W. H. Anion Exchange Resins for the Selective Separation of Technetium from Uranium in Carbonate Solutions. *Ind. Eng. Chem. Res.* **2012**, *51*, 10445−10450.
(19) Xie, R.; Shen, N.; Chen, X.; Li, J.; Wang, Y.; Zhang, C.; Xiao, C.; Chai, Z.; Wang, S. $^{99}TcO_4^-$ Separation through Selective Crystallization Assisted by Polydentate Benzene-Aminoguanidinium Ligands. *Inorg. Chem.* **2021**, *60*, 6463−6471.
(20) Weng, H.; Zhang, P.; Guo, Z.; Chen, G.; Shen, W.; Chen, J.; Zhao, X.; Lin, M. Efficient and Ultrafast Adsorption of Rhenium by Functionalized Hierarchically Mesoporous Silica: A Combined Strategy of Topological Construction and Chemical Modification. *ACS. Appl. Mater. Interfaces* **2021**, *13*, 8249−8262.
(21) Shan, W.; Zhang, Y.; Shu, Y.; Zhang, D.; Xing, C.; Xiong, Y. Enhanced Adsorption and Separation of Re(VII) Using Organic-Inorganic Hybrid Silica Adsorbent. *Microporous Mesoporous Mater.* **2021**, *317*, No. 110996.
(22) Shan, W.; Wang, D.; Zhang, Z.; Lou, Z.; Xiong, Y.; Fan, Y. Synthesis of Schiff Base-Functionalized Silica for Effective Adsorption of Re(VII) from Aqueous Solution. *J. Taiwan Inst. Chem. Eng.* **2019**, *100*, 277−284.
(23) Wang, S.; Alekseev, E. V.; Diwu, J.; Casey, W. H.; Phillips, B. L.; Depmeier, W.; Albrecht-Schmitt, T. E. NDTB-1: A Supertetrahedral Cationic Framework that Removes TcO_4^- from Solution. *Angew. Chem. Int. Ed.*. **2010**, *49*, 1057−1060.
(24) Wang, S.; Yu, P.; Purse, B. A.; Orta, M. J.; Diwu, J.; Casey, W. H.; Phillips, B. L.; Alekseev, E. V.; Depmeier, W.; Hobbs, D. T.; Albrecht-Schmitt, T. E. Selectivity, Kinetics, and Efficiency of Reversible Anion Exchange with TcO_4^- in a Supertetrahedral Cationic Framework. *Adv. Funct. Mater.* **2012**, *22*, 2241−2250.
(25) Wang, Y.; Gao, H. Compositional and Structural Control on Anion Sorption Capability of Layered Double Hydroxides (LDHs). *J. Colloid Interface Sci.* **2006**, *301*, 19−26.
(26) Sheng, G.; Tang, Y.; Linghu, W.; Wang, L.; Li, J.; Li, H.; Wang, X.; Huang, Y. Enhanced Immobilization of ReO_4^- by Nanoscale Zerovalent Iron Supported on Layered Double Hydroxide via an Advanced XAFS Approach: Implications for TcO_4^- Sequestration. *Appl. Catal., B* **2016**, *192*, 268−276.
(27) Sheng, D.; Zhu, L.; Dai, X.; Xu, C.; Li, P.; Pearce, C. I.; Xiao, C.; Chen, J.; Zhou, R.; Duan, T.; Farha, O. K.; Chai, Z.; Wang, S. Successful Decontamination of $^{99}TcO_4^-$ in Groundwater at Legacy Nuclear Sites by a Cationic Metal-Organic Framework with Hydrophobic Pockets. *Angew. Chem., Int. Ed.* **2019**, *58*, 4968−4972.
(28) Drout, R. J.; Otake, K.; Howarth, A. J.; Islamoglu, T.; Zhu, L.; Xiao, C.; Wang, S.; Farha, O. K. Efficient Capture of Perrhenate and Pertechnetate by a Mesoporous Zr Metal−Organic Framework and Examination of Anion Binding Motifs. *Chem. Mater.* **2018**, *30*, 1277−1284.
(29) Sheng, D.; Zhu, L.; Xu, C.; Xiao, C.; Wang, Y.; Wang, Y.; Chen, L.; Diwu, J.; Chen, J.; Chai, Z.; Albrecht-Schmitt, T. E.; Wang, S. Efficient and Selective Uptake of TcO_4^- by a Cationic Metal-Organic Framework Material with Open Ag^+ Sites. *Environ. Sci. Technol.* **2017**, *51*, 3471−3479.
(30) Zhu, L.; Sheng, D.; Xu, C.; Dai, X.; Silver, M. A.; Li, J.; Li, P.; Wang, Y.; Wang, Y.; Chen, L.; Xiao, C.; Chen, J.; Zhou, R.; Zhang, C.; Farha, O. K.; Chai, Z.; Albrecht-Schmitt, T. E.; Wang, S. Identifying the Recognition Site for Selective Trapping of $^{99}TcO_4^-$ in a Hydrolytically Stable and Radiation Resistant Cationic Metal-Organic Framework. *J. Am. Chem. Soc.* **2017**, *139*, 14873−14876.
(31) Li, J.; Wang, X.; Zhao, G.; Chen, C.; Chai, Z.; Alsaedi, A.; Hayat, T.; Wang, X. Metal-Organic Framework-Based Materials: Superior Adsorbents for the Capture of Toxic and Radioactive Metal Ions. *Chem. Soc. Rev.* **2018**, *47*, 2322−2356.
(32) Zhang, D.; Ronson, T. K.; Mosquera, J.; Martinez, A.; Nitschke, J. R. Selective Anion Extraction and Recovery Using a $Fe_4^{II}L_4$ Cage. *Angew. Chem., Int. Ed.* **2018**, *57*, 3717−3721.
(33) Banerjee, D.; Xu, W.; Nie, Z.; Johnson, L. E.; Coghlan, C.; Sushko, M. L.; Kim, D.; Schweiger, M. J.; Kruger, A. A.; Doonan, C. J.; Thallapally, P. K. Zirconium-Based Metal-Organic Framework for Removal of Perrhenate from Water. *Inorg. Chem.* **2016**, *55*, 8241−8243.
(34) Kang, K.; Liu, S.; Zhang, M.; Li, L.; Liu, C.; Lei, L.; Dai, X.; Xu, C.; Xiao, C. Fast Room-Temperature Synthesis of an Extremely Alkaline-Resistant Cationic Metal−Organic Framework for Sequestering TcO_4^- with Exceptional Selectivity. *Adv. Funct. Mater.* **2022**, *32*, No. 2208148.
(35) Fei, H.; Bresler, M. R.; Oliver, S. R. A New Paradigm for Anion Trapping in High Capacity and Selectivity: Crystal-to-Crystal Transformation of Cationic Materials. *J. Am. Chem. Soc.* **2011**, *133*, 11110−11113.
(36) Kang, K.; Dai, X.; Shen, N.; Xie, R.; Zhang, X.; Lei, L.; Wang, S.; Xiao, C. Unveiling the Uncommon Fluorescent Recognition Mechanism towards Pertechnetate Using a Cationic Metal-Organic Framework Bearing N-Heterocyclic AIE Molecules. *Chem. - Eur. J.* **2021**, *27*, 5632−5637.
(37) Kang, K.; Li, L.; Zhang, M.; Zhang, X.; Lei, L.; Xiao, C. Constructing Cationic Metal-Organic Framework Materials Based on Pyrimidyl as a Functional Group for Perrhenate/Pertechnetate Sorption. *Inorg. Chem.* **2021**, *60*, 16420−16428.
(38) Zhu, L.; Xiao, C.; Dai, X.; Li, J.; Gui, D.; Sheng, D.; Chen, L.; Zhou, R.; Chai, Z.; Albrecht-Schmitt, T. E.; Wang, S. Exceptional Perrhenate/Pertechnetate Uptake and Subsequent Immobilization by a Low-Dimensional Cationic Coordination Polymer: Overcoming the Hofmeister Bias Selectivity. *Environ. Sci. Technol. Lett.* **2017**, *4*, 316−322.
(39) Sun, Q.; Zhu, L.; Aguila, B.; Thallapally, P. K.; Xu, C.; Chen, J.; Wang, S.; Rogers, D.; Ma, S. Optimizing Radionuclide Sequestration in Anion Nanotraps with Record Pertechnetate Sorption. *Nat. Commun.* **2019**, *10*, No. 1646.

(40) Li, X.; Li, Y.; Wang, H.; Niu, Z.; He, Y.; Jin, L.; Wu, M.; Wang, H.; Chai, L.; Al-Enizi, A. M.; Nafady, A.; Shaikh, S. F.; Ma, S. 3D Cationic Polymeric Network Nanotrap for Efficient Collection of Perrhenate Anion from Wastewater. *Small* **2021**, *17*, No. 2007994.
(41) Liu, Z. W.; Han, B. H. Evaluation of an Imidazolium-Based Porous Organic Polymer as Radioactive Waste Scavenger. *Environ. Sci. Technol.* **2020**, *54*, 216−224.
(42) Samanta, P.; Chandra, P.; Dutta, S.; Desai, A. V.; Ghosh, S. K. Chemically Stable Ionic Viologen-Organic Network: an Efficient Scavenger of Toxic Oxo-Anions from Water. *Chem. Sci.* **2018**, *9*, 7874−7881.
(43) Li, J.; Dai, X.; Zhu, L.; Xu, C.; Zhang, D.; Silver, M. A.; Li, P.; Chen, L.; Li, Y.; Zuo, D.; Zhang, H.; Xiao, C.; Chen, J.; Diwu, J.; Farha, O. K.; Albrecht-Schmitt, T. E.; Chai, Z.; Wang, S. $^{99}TcO_4^-$ remediation by a cationic polymeric network. *Nat. Commun.* **2018**, *9*, No. 3007.
(44) Ding, M.; Chen, L.; Xu, Y.; Chen, B.; Ding, J.; Wu, R.; Huang, C.; He, Y.; Jin, Y.; Xia, C. Efficient Capture of Tc/Re(VII, IV) by a Viologen-Based Organic Polymer Containing Tetraaza Macrocycles. *Chem. Eng. J.* **2020**, *380*, No. 122581.
(45) Li, J.; Chen, L.; Shen, N.; Xie, R.; Sheridan, M. V.; Chen, X.; Sheng, D.; Zhang, D.; Chai, Z.; Wang, S. Rational Design of a Cationic Polymer Network Towards Record High Uptake of $^{99}TcO_4^-$ in Nuclear Waste. *Sci. China Chem.* **2021**, *64*, 1251−1260.
(46) Li, J.; Li, B.; Shen, N.; Chen, L.; Guo, Q.; Chen, L.; He, L.; Dai, X.; Chai, Z.; Wang, S. Task-Specific Tailored Cationic Polymeric Network with High Base-Resistance for Unprecedented $^{99}TcO_4^-$ Cleanup from Alkaline Nuclear Waste. *ACS Cent. Sci.* **2021**, *7*, 1441−1450.
(47) Da, H. J.; Yang, C. X.; Yan, X. P. Cationic Covalent Organic Nanosheets for Rapid and Selective Capture of Perrhenate: An Analogue of Radioactive Pertechnetate from Aqueous Solution. *Environ. Sci. Technol.* **2019**, *53*, 5212−5220.
(48) Hao, M.; Chen, Z.; Yang, H.; Waterhouse, G. I. N.; Ma, S.; Wang, X. Pyridinium Salt-Based Covalent Organic Framework with Well-Defined Nanochannels for Efficient and Selective Capture of Aqueous $^{99}TcO_4^-$. *Sci. Bull.* **2022**, *67*, 924−932.
(49) Chen, X.-R.; Zhang, C.-R.; Jiang, W.; Liu, X.; Luo, Q.-X.; Zhang, L.; Liang, R.-P.; Qiu, J.-D. 3D Viologen-Based Covalent Organic Framework for Selective and Efficient Adsorption of ReO_4^-/TcO_4^-. *Sep. Purif. Technol.* **2023**, *312*, No. 123409.
(50) Wang, Z.; Yang, J.; Cao, J.; Chen, W.; Wang, G.; Liao, F.; Zhou, X.; Zhou, F.; Li, R.; Yu, Z. Q.; Zhang, G.; Duan, X.; Wu, Y. Room-Temperature Synthesis of Single Iron Site by Electrofiltration for Photoreduction of CO_2 into Tunable Syngas. *ACS Nano* **2020**, *14*, 6164−6172.
(51) Zhang, C. R.; Cui, W. R.; Yi, S. M.; Niu, C. P.; Liang, R. P.; Qi, J. X.; Chen, X. J.; Jiang, W.; Liu, X.; Luo, Q. X.; Qiu, J. D. An Ionic Vinylene-Linked Three-Dimensional Covalent Organic Framework for Selective and Efficient Trapping of ReO_4^- or $^{99}TcO_4^-$. *Nat. Commun.* **2022**, *13*, No. 7621.
(52) Hao, M.; Liu, Y.; Wu, W.; Wang, S.; Yang, X.; Chen, Z.; Tang, Z.; Huang, Q.; Wang, S.; Yang, H.; Wang, X. Advanced Porous Adsorbents for Radionuclides Elimination. *EnergyChem* **2023**, No. 100101.
(53) Kang, K.; Shen, N.; Wang, Y.; Li, L.; Zhang, M.; Zhang, X.; Lei, L.; Miao, X.; Wang, S.; Xiao, C. Efficient Sequestration of Radioactive $^{99}TcO_4^-$ by a Rare 3-fold Interlocking Cationic Metal-Organic Framework: A Combined Batch Experiments, Pair Distribution Function, and Crystallographic Investigation. *Chem. Eng. J.* **2022**, *427*, No. 130942.
(54) He, L.; Liu, S.; Chen, L.; Dai, X.; Li, J.; Zhang, M.; Ma, F.; Zhang, C.; Yang, Z.; Zhou, R.; Chai, Z.; Wang, S. Mechanism Unravelling for Ultrafast and Selective $^{99}TcO_4^-$ Uptake by a Radiation-Resistant Cationic Covalent Organic Framework: A Combined Radiological Experiment and Molecular Dynamics Simulation Study. *Chem. Sci.* **2019**, *10*, 4293−4305.
(55) Xie, Y.; Wu, Y.; Liu, X.; Hao, M.; Chen, Z.; Waterhouse, G. I. N.; Wang, X.; Yang, H.; Ma, S. Rational Design of Cooperative Chelating Sites on Covalent Organic Frameworks for Highly Selective Uranium Extraction from Seawater. *Cell Rep. Phys. Sci.* **2023**, *4*, No. 101220.
(56) Ameduri, B.; Bongiovanni, R.; Malucelli, G.; Pollicino, A.; Pripla, A. New Fluorinated Acrylic Monomers for the Surface Modification of UV-Curable Systems. *J. Polym. Sci., Part A: Polym. Chem.* **1999**, *37*, 77−87.
(57) Xiong, P.; Lu, D.; Chen, P.; Huang, L. S. H.; Guan, R. Characterization of acrylic copolymer latex modified by fluorine, silicon, and epoxy resin. *e-Polym.* **2008**, *8*, No. 047.
(58) Thomas, O. D.; Soo, K. J.; Peckham, T. J.; Kulkarni, M. P.; Holdcroft, S. A stable hydroxide-conducting polymer. *J. Am. Chem. Soc.* **2012**, *134*, 10753−10756.
(59) Fan, J.; Wright, A. G.; Britton, B.; Weissbach, T.; Skalski, T. J. G.; Ward, J.; Peckham, T. J.; Holdcroft, S. Cationic Polyelectrolytes, Stable in 10 M KOH(aq) at 100 degrees C. *ACS Macro Lett.* **2017**, *6*, 1089−1093.
(60) Langmuir, I. The Adsorption of Gases on Plane Surfaces of Glass, Mica and Platinum. *J. Am. Chem. Soc.* **1918**, *40*, 1361−1403.
(61) Xie, Y.; Liang, J.; Fu, Y.; Huang, M.; Xu, X.; Wang, H.; Tu, S.; Li, J. Hypercrosslinked Mesoporous Poly(ionic liquid)s with High Ionic Density for Efficient CO_2 Capture and Conversion into Cyclic carbonates. *J. Mater. Chem. A* **2018**, *6*, 6660−6666.
(62) Kunde, T.; Nieland, E.; Schroder, H. V.; Schalley, C. A.; Schmidt, B. M. A Porous Fluorinated Organic [4+4] Imine Cage Showing CO_2 and H_2 Adsorption. *Chem. Commun.* **2020**, *56*, 4761−4764.
(63) Wei, C.; Yang, Z.; Zhang, J.; Ji, H. Selective and Efficient Removal of ReO_4^- from Aqueous Solution by Imidazolium-based Porous Organic Polymers. *Colloids Surf., A* **2022**, *651*, No. 129754.
(64) Vilela, S. M. F.; Fernandes, J. A.; Ananias, D.; Carlos, L. D.; Rocha, J.; Toméb, J. P. C.; Paz, F. A. A. Photoluminescent Layered Lanthanide−Organic Framework Based on a Novel Trifluorotriphosphonate Organic Linker. *CrystEngComm* **2014**, *16*, 344−358.
(65) Zhang, Z.; Wu, C.; Pan, Q.; Shao, F.; Sun, Q.; Chen, S.; Li, Z.; Zhao, Y. Interfacial Synthesis of Crystalline Two-dimensional Cyanographdiyne. *Chem. Commun.* **2020**, *56*, 3210−3213.
(66) Shen, N.; Yang, Z.; Liu, S.; Dai, X.; Xiao, C.; Taylor-Pashow, K.; Li, D.; Yang, C.; Li, J.; Zhang, Y.; Zhang, M.; Zhou, R.; Chai, Z.; Wang, S. $^{99}TcO_4^-$ Removal from Legacy Defense Nuclear Waste by an Alkaline-Stable 2D Cationic Metal Organic Framework. *Nat. Commun.* **2020**, *11*, No. 5571.

https://doi.org/10.1021/acs.est.3c02967
Environ. Sci. Technol. 2023, 57, 10870−10881